

# Ion reflection at the shock front revisited

M. Gedalin

Department of Physics, Ben-Gurion University, Beer-Sheva, Israel

## 1. 1. Introduction

It is well known that reflected ions are responsible for at least a part of the supercritical collisionless shock structure, as well as for the dissipation in it (see for review, *Gosling and Robson* [1985, and references therein]). These reflected ions have been shown to be responsible for the magnetic foot formation ahead of the main magnetic ramp [*Woods*, 1971]. While the presence of these ions and their increasing role with the increase of the Mach number [*Gosling and Robson*, 1985] are very well established, the mechanism of the reflection is not understood in full detail (see, for example, *Burgess et al.* [1989]). At the same time, the details of the reflection mechanism should determine what part of the initial distribution is reflected and what is the spatial and phase-space distribution of the reflected ions. In particular, the behavior of reflected ions determines the foot length, which is used for the determination of the shock-spacecraft closing velocity when two spacecraft measurements are unavailable [*Gosling and Thomsen*, 1985]. There may be also implications for the behavior of pickup ions at interplanetary and termination shocks and for the ion injection for subsequent Fermi acceleration (see, for example, *Lee et al.* [1995]).

*Woods* [1971] proposed a model of specular reflection which has been extensively exploited since then (see *Wilkinson and Schwartz* [1990, and references therein]). The model predicts formation of a well-defined ion semiring in the foot and the turnaround distance (which is also the foot length) of  $d_{\text{foot}} = 0.68(V_u/\Omega_u)$  in the perpendicular geometry, where  $V_u$  is the solar wind velocity (upstream plasma velocity) and  $\Omega_u = eB_u/m_i$  is the upstream ion gyrofrequency. (Generalization of the expression for the foot length in general oblique geometry has been done by *Gosling and Thomsen* [1985].)

Observations [*Sckopke et al.*, 1983] (measurements of the foot length, ion gyration velocities at the outer edge of the foot, and gyration velocities of the ions which have been reflected and afterward transmitted into the downstream region) showed order-of-magnitude agreement with the model. To explain the upstream reflected ion population, which is much more diffuse than the predicted beam of specular reflected ions, specular reflection+isotropic scattering at the ramp was proposed. Later studies (observational [*Scudder et al.*, 1986a; *Gosling and Thomsen*, 1985] and numerical [*Burgess et al.*, 1989]) revealed substantial discrepancy (often by a factor  $> 2$ ) between the predicted and measured foot length. Numerical analysis [*Burgess et al.*, 1989] has shown that the reflection process is very sensitive to the initial conditions (ion velocities at the upstream edge of the ramp) and the core ions are not reflected at all, while the reflection of the tail ions depends strongly on the initial gyrophase. Incorporating reflected ions into the shock structure description within the specular reflection model, *Wilkinson and Schwartz* [1990] found that the cross-shock potential increases rapidly with the increase of the Mach number, until it achieves the constant value  $e\varphi = m_i V_u^2 / 2$ , which is well above of what is measured [*Scudder et al.*, 1986a] and found in hybrid simulations [*Goodrich*, 1985]. This is at odds with the known anti-correlation between the cross-shock potential and the number of reflected ions: the latter increases with the increase of the Mach number, while the former decreases [*Gosling and Robson*, 1985; *Goodrich*, 1985].

*Leroy* [1983] proposed that the magnetic forces in the foot sufficiently augment the electric forces to cause ion reflection at the ramp. It was found that the magnetic field should double over the whole foot to provide necessary slowing down. Hybrid simulations [*Burgess et al.*, 1989] showed, on the other hand, that the largest effect of the magnetic field increase in the foot is the bulk acceleration of the incident ion beam in the negative direction of  $y$  axis. Ions were not stopped at the ramp, but began to acquire negative  $u_x$  near or at the potential maximum in the overshoot, well beyond the ramp.

The objective of the present paper is to study the details of the ion reflection process and to determine the physical mechanism and the shock parameters which control the ion reflection. Our approach differs significantly from the earlier models in that we do not assume electrostatic braking but directly analyze what happens with an ion in the structured shock front (foot, ramp, and overshoot). The paper is organized as follows. In section 2 we analyze the ion motion in the general stationary perpendicular shock structure, paying special attention to the role of the different parts of the shock structure. We develop an approximation for the description of the reflection process and derive the reflection condition as a function of the shock parameters. In contrast with the analysis of *Leroy* [1983] we consider the single-particle behavior in the already established stationary field profiles of the shock, which allows us to get rid of the assumption of cold ion beams and make estimates using parameters of observed and simulated shocks. In section 3 we perform a test particle numerical analysis of the ion motion in the model shock front. The parameters of the shock structure are taken close to the parameters of the high-Mach number supercritical shock, described by *Scudder et al.* [1986a]. The test particle analysis has a shortcoming in comparison with, for example, hybrid simulations, in that the former does not describe the shock self-consistently. On the other hand, it has its own advantages. Once the shock field structure is established, the particle motion in it is fully determined by the electric and magnetic fields, so that initial conditions for the analyzed trajectory can be chosen arbitrarily. Diagnostics is also much easier. Scales of the order of  $c/\omega_{pe}$  which are absent in hybrid simulations

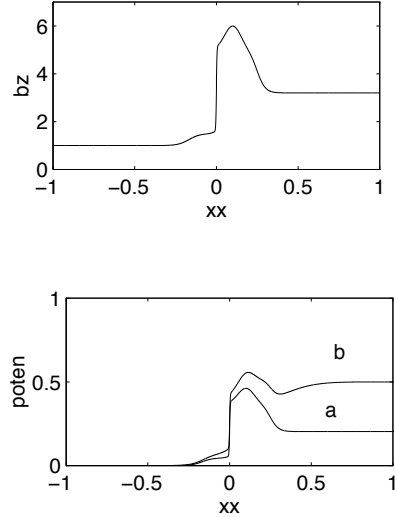


**Figure 1.** The (a) magnetic field and (b) electric potential profiles of a supercritical shock. The magnetic field and scale parameters for this figure are taken close to those of *Scudder et al.* [1986a]. The potential is shown for the case when there is only electric field corresponding to (1) (total cross-shock potential  $e\varphi_t = 0.2(m_i V_u^2/2)$ ) and when there is an additional superimposed electric field which ensures  $e\varphi_t = 0.5(m_i V_u^2/2)$ .

but present in observations can be easily included in the prescribed field profile. At last, irreversible processes (such as, for example, instabilities and wave-particle interaction) are not included. This is a shortcoming, since nothing can smooth out highly nonequilibrium distributions. On the other hand, this allows to study the reversible effects in their pure form. Our test particle analysis illustrates the applicability of the analytical approach developed in section 2 and also provides some quantitative estimates which cannot be obtained otherwise because of mathematical difficulties.

## 2. 2. Ion Motion in the Perpendicular Shock

In what follows, we rely on the following qualitative shock picture, which was found both in observations [*Scudder et al.*, 1986a] and simulations [*Goodrich*, 1985]. The one-dimensional stationary shock front consists of the extended foot with the length  $L_f \sim 0.5(V_u/\Omega_u)$ , narrow ramp with  $c/\omega_{pi} > L_r > c/\omega_{pe}$ , overshoot with  $L_o \sim V_u/\Omega_d = (V_u/\Omega_u)/(B_d/B_u)$ , and downstream region (probably containing smaller undershoots and overshoots). The electric potential is distributed over the wide region including foot, ramp, and overshoot and penetrates deeply into the downstream region, so that only a part of the total cross-shock potential is applied at the foot and ramp.

Working in a perpendicular geometry we assume that the shock normal is along  $x$  axis, the magnetic field is along  $z$  axis, and the constant motional electric field  $E_y = V_u B_u$ . A more or less typical magnetic field profile of a supercritical shock is shown in Figure 1a for the set of parameters taken close to that of *Scudder et al.* [1986a]. The shock Mach number  $M = 7.5$ , the downstream to upstream magnetic compression ratio  $B_d/B_u = 3.2$ , the magnetic field at the ramp increases up to  $B_r \approx 5B_u$ , and at the overshoot  $B_o = 6B_u$ . The foot length is  $\approx 0.3(V_u/\Omega)$  and the ramp width  $\approx 0.2(c/\omega_{pi})$ . The magnetic field increases by  $\approx 50\%$  at the foot.

While the high-resolution magnetic profile of a shock is quite well known, the electric field is known with much less confidence. We use a rough approximation of a simple two-fluid hydrodynamics which reads

$$E_x = -\frac{1}{2\mu_0 en} \frac{B^2}{dx} - \frac{1}{en} \frac{dp_e}{dx}, \quad (1)$$

where  $p_e$  is the electron pressure, which is assumed isotropic. Actual electric field deviates from this form due to nonnegligible ion current (see, for example, discussion by *Goodrich* [1985]). Although (1) is not correct, generally speaking, it describes properly the weakness of the potential electric field in the foot and the sharp electric field peak in the ramp [cf. *Wygant et al.*, 1987; *Liewer et al.*, 1991]. As we shall see below, the part of the potential which penetrates deeply into the downstream region [*Scudder et al.*, 1986a, b], does not affect much the ion reflection. The exact form of the electric field in the ramp is unimportant either. We shall therefore use (1) as a convenient approximation for the shock potential electric field in the foot, ramp, and a part of the overshoot, remembering that the actual field may be different and there may be an

additional (probably weak) electric field which penetrates deeply to the downstream region. We shall also use the approximations  $n \propto B$  and  $p_e \propto n^{\gamma_e}$  [cf. *Scudder et al.*, 1986a]. In our case,  $\beta_e = 1.6$  and  $\gamma_e = 2$ . The electric field determined by (1) is consistent with the field observed numerically (cf. *Burgess et al.* [1989, Figure 4]). The maximum electric field at the ramp estimated from (1) is also consistent with the value reported by *Scudder et al.* [1986a] in Figure 3. Exact shape of the electric field is not especially important for the present analysis, as we shall see below. The total cross-shock potential found by *Scudder et al.* [1986a] is substantially larger than ours but is obtained by approximating the electric field by Gaussian which penetrates deeply into the downstream region; a substantial part of this potential belongs to the region well beyond the ramp and overshoot. In the numerical study in section 3 we analyze also the effect of this additional field.

The ion motion in the perpendicular shock is described by the following equations:

$$\dot{u}_x = (e/m_i)E_x + (e/m_i)u_yB_z, \quad (2)$$

$$\dot{u}_y = (e/m_i)E_y - (e/m_i)u_xB_z. \quad (3)$$

It does not seem possible to solve these equations in general case. However, they can be analyzed approximately in our case, because of the fact that the ions spend only  $\sim 0.1$  of their gyroperiod in the foot and ramp. In what follows, we generalize the consideration of *Leroy* [1983], directly analyzing ion motion in the electromagnetic field of the shock in the foot, ramp, and overshoot.

We consider first the ion motion before it is stopped or reached a turning point  $u_x = 0$ . In this case,  $u_x > 0$ , and we can substitute  $(d/dt) = u_x(d/dx)$  in (2) and (3), which take the following form:

$$\frac{d}{dx}\left(\frac{u_x^2}{2} + \frac{e\varphi}{m_i}\right) = \Omega u_y, \quad (4)$$

$$\frac{d}{dx}u_y = \Omega_u \frac{V_u}{u_x} - \Omega, \quad (5)$$

where we have introduced the electrostatic potential  $E_x = -d\varphi/dx$ , and  $\Omega = \Omega(x) = eB_z/m_i$ . (5) immediately gives

$$u_y = v_y + \int_{x_0}^x d\xi \left( \Omega_u \frac{V_u}{u_x(\xi)} - \Omega(\xi) \right), \quad (6)$$

where the initial conditions are  $(u_x, u_y) = (v_x, v_y)$  at  $x = x_0$ . Substituting (6) into (4) and integrating, one obtains

$$\begin{aligned} u_x^2 &= v_x^2 - \frac{2e\varphi(x)}{m_i} + 2v_y \int_{x_0}^x d\xi \Omega(\xi) \\ &\quad - 2 \int_{x_0}^x d\xi_1 \Omega(\xi_1) \int_{x_0}^{\xi_1} d\xi \left( \Omega_u \frac{V_u}{u_x(\xi)} - \Omega(\xi) \right). \end{aligned} \quad (7)$$

The second and third terms in (7) are responsible for the ion deceleration due to the magnetic forces and can be described as additional potentials. Let us now for convenience completely distinguish the foot (length  $L_f$ , monotonically increasing magnetic field from  $B_u$  to  $B_f$ ), ramp (length  $L_r$ , monotonically increasing magnetic field from  $B_f$  to  $B_r$ ), and overshoot (length  $L_o$ , the largest magnetic field  $B_o$ ), although the real transitions are smooth.

## 2.1. Foot

The  $y$  deflection of the ion is estimated as

$$\delta u_{y,f} = \frac{\Omega_u L_f}{v_x} - \int_0^{L_f} \Omega(x) dx, \quad (8)$$

where we neglected the deceleration in  $x$  direction, assuming  $e\varphi_f \sim 0.1(m_i V_u^2/2)$ . When  $v_T/V_u = \sqrt{\beta_i/2}/M \ll 1$ , (8) can be estimated as  $\delta u_{y,f} \approx (\Omega_f - \Omega_u)L_f/2 \approx 0.08$  in our case. Substitution of (8) with  $v_y \sim v_T$  in (7) for  $B_f \approx 1.5B_u$ ,  $L_f \approx 0.3(V_u/\Omega_u)$ ,  $\beta_i = 0.8$ , and  $M \approx 7.5$  [*Scudder et al.*, 1986a] gives the effective addition to the potential of about  $|e\varphi_1| < 0.05(m_i V_u^2/2)$ . Therefore an ion comes to the ramp slightly decelerated and noticeably deflected [cf. *Leroy*, 1983] in  $y$  direction.

## 2.2. Ramp

Equations (4)-(5) are valid in the ramp also, as long as the ion is not completely decelerated and stopped [*Burgess et al.*, 1989]. The deceleration in  $x$  direction in this region is determined mainly by the potential  $e\varphi_r \sim 0.5(m_i V_u^2/2)$  and is strong, while the upper limit on the deflection in  $y$ -direction can be estimated by substituting  $u_x = V_u$  in (5), which gives

$$\begin{aligned} \delta u_{y,r} &= \int_{L_f}^{L_f+L_r} (\Omega(x) - \Omega_u) dx \\ &\approx (B_f + B_r - 2B_u)L_r/2 \approx 0.04V_u \end{aligned} \quad (9)$$

in our case. The lower limit  $\approx 0.03V_u$  is estimated by substituting  $u_x = (V_u^2 - 2e\varphi_r/m_i)^{1/2}$  in (5).

### 2.3. Foot and Ramp Together

Summarizing all the above, we approximate the ion velocity at the downstream edge of the ramp as follows:

$$w_x = (v_x^2 - 2e\varphi_r/m_i)^{1/2}, \quad w_y = v_y - V_s, \quad (10)$$

where  $\varphi_r$  is the potential at the end of the ramp and  $V_s$  is the velocity shift in  $y$  direction due to the gradual increase of the magnetic field of the foot and finite (nonzero) width of the ramp. In general, this shift depends on  $(v_x, v_y)$ . However, for  $v_T/V_u \ll 1$  this dependence is weak, and  $V_s$  can be estimated as

$$V_s \approx (B_f - B_u)L_f/2 + (B_f + B_r - 2B_u)L_r/2. \quad (11)$$

It should be emphasized that the above expressions are approximate and valid only if  $u_x$  is not too small. The number of ions which are strongly decelerated to  $u_x \approx 0$  is small if  $(V_u^2 - 2e\varphi_r/m_i) \gtrsim 3v_T$ , which is not satisfied for  $\beta_i \gg 1$  or  $e\varphi_r \approx m_i V_u^2/2$ . Ions which are strongly decelerated require more precise treatment since they spent much time in the ramp.

### 2.4. Overshoot

In the overshoot the relative variation of the magnetic field  $(B_o - B_r)/B_r \sim 0.2 \ll 1$ , so that we approximate  $B = B_r = RB_u = \text{const}$ . The electric field in the overshoot can be estimated as  $-(\varphi_o - \varphi_r)/L_o \approx \text{const}$ , or using (1), as follows:

$$\frac{E_o}{E_y} \approx -\frac{1}{M^2} \left(2 + \gamma_e \beta_e \left(\frac{B_r}{B_u}\right)^{\gamma_e-1}\right) \frac{B_o - B_r}{L_o/(V_u/\Omega_u)}. \quad (12)$$

For the parameters above and the overshoot length of

$0.15V_u/\Omega_u$  one finds  $E_o \approx -0.6E_y$ . Although this electric field is not strong, it is important as we shall see below.

Substituting these fields into (2) and (3), it is easy to find the general solution in the form

$$u_x = V_r + v_\perp \cos(\Omega_r t - \alpha), \quad (13)$$

$$u_y = V_{sh} - v_\perp \sin(\Omega_r t - \alpha), \quad (14)$$

$$x = V_r t + v_\perp \sin(\Omega_r t - \alpha)/\Omega_r + v_\perp \sin \alpha / \Omega_r, \quad (15)$$

where  $V_r = V_u/R$ ,  $\Omega_r = R\Omega_u$ ,  $x = 0$  is the coordinate of the downstream edge of the ramp,  $V_{sh} = E_o/B_r$ , and

$$v_\perp^2 = (w_x - V_r)^2 + (w_y - V_{sh})^2, \quad (16)$$

$$\alpha = \arcsin((w_y - V_{sh})/v_\perp).$$

It is easy to see that an ion is reflected, that is, crosses back the ramp to the upstream, when the following conditions are satisfied:  $\exists t_0 > 0$  so that  $u_x(t_0) = 0$ ,  $u_y(t_0) > 0$ , and  $x(t_0) < 0$ . Hence the reflection condition can be written in the following form:

$$v_\perp \sin \alpha + V_r [\pi + \alpha + \arccos(V_r/v_\perp)] - (v_\perp^2 - V_r^2)^{1/2} < 0, \quad (17)$$

For the returning ion at the downstream edge of the ramp from (14) and (15) one has

$$u_y^{(b)} = w_y + V_r [\pi + \alpha + \arcsin(\frac{u_y^{(b)} - V_{sh}}{v_\perp})], \quad (18)$$

from which we see that  $u_y^{(b)} > w_y$  always.

Equation (17) shows that the chances of an ion to be reflected (to come back to the ramp) are higher when  $v_\perp$  is larger. The ions with larger  $v_\perp$  also move farther upstream from the ramp and thus determine the foot length. For these ions one may assume  $(w_y - V_{sh})/v_\perp, V_r/v_\perp, (u_y - V_s)/v_\perp \ll 1$  and solve (18) to obtain approximately

$$u_y^{(b)} \approx w_y + V_r (w_y - V_{sh})/v_\perp + V_r \{\pi + \arcsin[(w_y - V_{sh})/v_\perp]\}, \quad (19)$$

$$u_x^{(b)} \approx V_r - v_\perp [1 - (u_y^{(b)} - V_{sh})^2/2v_\perp^2]. \quad (20)$$

To estimate the ion velocity  $(u_x^{(r)}, u_y^{(r)})$  at the upstream edge of the ramp, we follow the thin ramp approximation by Leroy [1983] to obtain

$$u_x^{(r)} = -[(u_x^{(b)})^2 + 2e\varphi_r/m_i]^{1/2}, \quad u_y^{(r)} = u_y^{(b)}, \quad (21)$$

### 2.5. Foot Again: Turnaround Distance

It does not seem possible to solve the equations of motion for gyrating ions in the spatially varying magnetic field of the foot. We shall estimate the turnaround distance (and the foot length) by putting  $B = B_u = \text{const}$  and allowing for further modification by substituting  $B \rightarrow \langle B \rangle_{\text{foot}}$ , as proposed by *Sckopke et al.* [1983]. In the constant magnetic field the determination of the turnaround point is straightforward and described in detail by *Woods* [1971] (see also *Schwartz et al.* [1983]). We present only the result. The distance of the turnaround point where  $u_x = 0$  from the upstream edge of the ramp is

$$\begin{aligned} d/(V_u/\Omega_u) &= (w_\perp^2/V_u^2 - 1)^{1/2} \\ &+ [\phi - \arccos(V_u/w_\perp)] - u_y^{(r)}/V_u, \\ w_\perp^2 &= (u_x^{(r)} - V_u)^2 + (u_y^{(r)})^2, \\ \phi &= \arcsin(u_y^{(r)}/w_\perp). \end{aligned} \quad (22)$$

In the turnaround point,  $u_y^{(T)} = (w_\perp^2 - V_u^2)^{1/2}$ .

### 2.6. Nonspecular Reflection: Summary

To summarize, we developed a model in which the reflection condition depends on four parameters: magnetic compression ratio  $B_r/B_u$  at the ramp, relative potential at the ramp  $e\varphi_r/(m_i V_u^2/2)$ , shift velocity  $V_s/V_u$  due to the increase of the magnetic field, and effective shift velocity  $V_{sh}/V_u$  due to the electric field in the overshoot. The first two parameters are characteristics of the shock structure only. The third and fourth parameters depend, generally speaking, on the initial ion velocity also, but in the high Mach number shocks this dependence is weak because of  $v_T/V_u \ll 1$ .

Given all these parameters, the turnaround distance of an ion is the function of its initial velocity. To estimate the foot length, let us define for the present paper that the measure of the foot corresponds to the largest turnaround distance of an ion taken from the distribution where the relative phase space density is 0.01, that is,  $f(v_x, v_y) = 0.01f(V_u, 0)$ . Since (17) shows that  $v_\perp$  should be as large as possible, while  $v_y$  should be as negative as possible (in this case the above approximations also work better and better), we conclude that the turnaround distance of the ion with the initial velocity  $(V_u + 2.15v_T, -2.15v_T)$  can be used as a measure of the foot length. Since (17) and (22) show clear dependence on the initial velocity of the ion, one can expect that the foot length will significantly depend on  $\beta_i$  also. For our model parameters this gives  $d_{\text{foot}} \approx 0.4(V_u/\Omega_i)$  when we neglect the increase of the magnetic field, or  $d_{\text{foot}} \approx 0.3(V_u/\Omega_i)$  if we use the mean magnetic field  $\langle B \rangle = (B_u + B_f)/2$  in (22). This estimate is consistent with the assumed foot length, observations [*Scudder et al.*, 1986a], and hybrid simulations [*Burgess et al.*, 1989].

## 3. 3. Numerical Analysis

In order to illustrate the theoretical analysis and to study the features, which cannot be studied theoretically at present, we perform a numerical analysis of the ion reflection. We trace test particles (ions) through the shock field structure, described in section 2. The following analytical expression has been chosen to describe the magnetic field profile presented in Figure 1a:

$$\begin{aligned} \frac{B_z}{B_u} &= 1 + \frac{R_f - 1}{2}(1 + \tanh \frac{3(x + D_f - 3D_r)}{D_f}) \\ &+ \frac{R_r - R_f}{2}(1 + \tanh \frac{3x}{D_r}) \\ &+ (R_o - R_r) \exp(-\frac{2(x - D_o)^2}{D_o^2}) \\ &+ \frac{R_d - R_r}{2}(1 + \tanh \frac{3(x - D_o - D_d)}{D_d}), \end{aligned} \quad (23)$$

where  $R_f = 1.5$ ,  $R_r = 5$ ,  $R_o = 6$ ,  $R_d = 3.2$ ,  $D_f = 0.3$ ,  $D_r = 0.01$ ,  $D_o = 0.1$ , and  $D_d = 0.15$  provide the necessary scales. The electric field, which is actually the electric field of the foot, ramp, and overshoot (partly), is found from (1), if not stated otherwise. In several cases we superimpose an additional electric field distributed over a much wider region, to explicitly control the total cross-shock potential  $\varphi_t$  (see Figure 1b).

All ion trajectories start at the edge of the foot  $x_{\text{in}} = -0.3(V_u/\Omega_u)$  and are traced to the downstream region in the prescribed electric and magnetic fields. The initial ion distribution is Maxwellian with  $\beta_i = 0.8$ . Trajectories  $u_x(x)$  and  $u_y(x)$  for 50 ions are shown together in Figure 2. Since the number of counts in any given (small) space interval  $\Delta x$  is proportional to the crossing time, plotting all trajectories  $(x, u_x)$  and  $(x, u_y)$  together is equivalent to the staying time method and Figures 2a and 2b represent the ion phase space in the steady state. They do not contain much new information

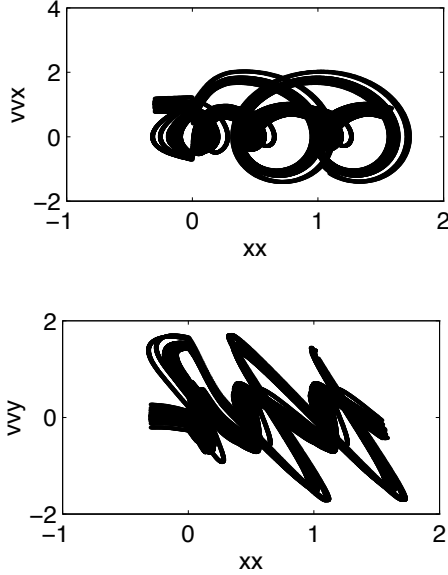


**Figure 2.** Ion phase space in the steady state obtained from trajectories of 50 ions.

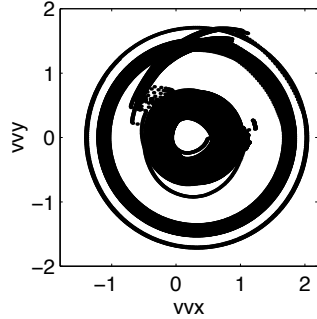


**Figure 3.** Projected ion velocity space.

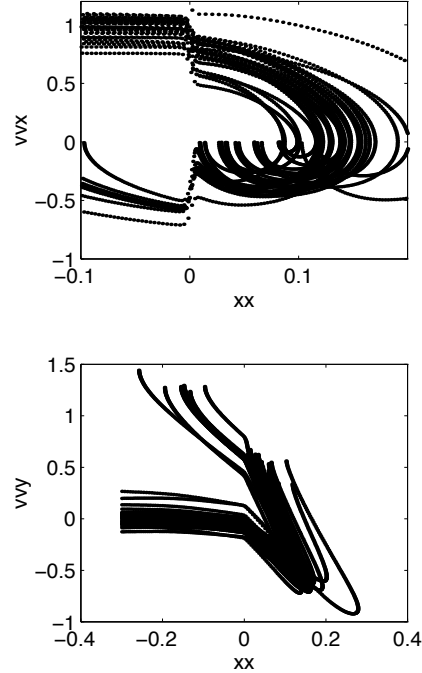
but show consistency of our results with the results of more sophisticated simulations (cf., for example, [Burgess *et al.*, 1989, Figure 1]), and also the power and convenience of the trajectory analysis. From Figure 2b it is also clearly seen that the ions, crossing the ramp from downstream to upstream, have substantial  $u_y > 0$ . Figure 2 also shows that the turnaround distances of the ions are consistent with the foot length, chosen in the model.

Figure 3 shows the projection of the three-dimensional space  $R^3[x, u_x, u_y]$ , containing 50 traced trajectories, onto the ion velocity space  $(u_x, u_y)$ . The outer ring in this velocity space corresponds to the ions that have been reflected and transmitted to the downstream region at their second encounter with the ramp. These ions are situated at a circle with a radius slightly less than  $2V_u$  around the downstream fluid velocity, in perfect agreement with observations [Sckopke *et al.*, 1983].

Figure 4 provides more detailed qualitative information about the reflection process. All reflected ions penetrate significantly into the overshoot, so that the first turning point, where  $u_x = 0$ , is beyond the ramp [cf. Burgess *et al.*, 1989]. Yet the total potential drop, which an ion crosses, remains substantially less than  $m_i v_x^2 / 2$ . The ion deceleration in  $x$  direction in the foot is relatively weak, while the deflection in  $y$  direction is quite noticeable. The main drop of  $u_x$  occurs at the ramp. The ions with relatively low  $v_\perp$  (see (16)) just behind the ramp are convected downstream and do not return to the ramp. On the other hand, ions which have sufficiently high  $v_\perp$  at the downstream edge of the ramp do return back to the ramp (depending on their initial gyrophase, determined by  $u_y$ ), cross it and appear as reflected-gyrating ions in the foot.

Because of the considerable time spent by the reflected ions in the overshoot, the velocity dispersion of the returning ions at the ramp is substantial and the corresponding reflected ion distribution in the foot is much more diffuse than could be expected if the reflection was specular. The component  $u_y$  of the returning ion at the ramp controls the initial gyrophase of the reflected-gyrating ion in the foot and therefore the distance at which the ion turns back to the ramp again. Substantial  $u_y > 0$  results in smaller turnaround distances and foot lengths than could be expected if the reflection was specular.

In Figure 5 we show the part of the ion distribution which is reflected, as obtained from the numerical analysis (crosses) and predicted by (17) (open circles) for 200 traced ions. The difference between Figures 5a and 5b is in the potential: in the



**Figure 4.** Trajectories of 30 ions traced up to the turnaround point where  $u_x = 0$  and  $u_y > 0$ .

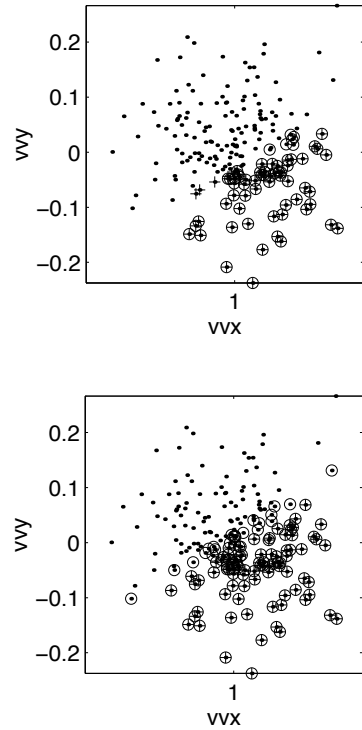


**Figure 5.** Initial velocities of the reflected ions. Points correspond to the initial Maxwellian distribution at the outer edge of the foot. Open circles mark those of them which are reflected according to the analytical model proposed in section 2. Crosses mark those reflected ions which were observed in the numerical analysis. (a) Corresponds to the potential obtained from (1), while (b) in there is an additional electric field, distributed over a wide region, so that  $e\varphi_t = 0.5(m_i V_u^2 / 2)$ .

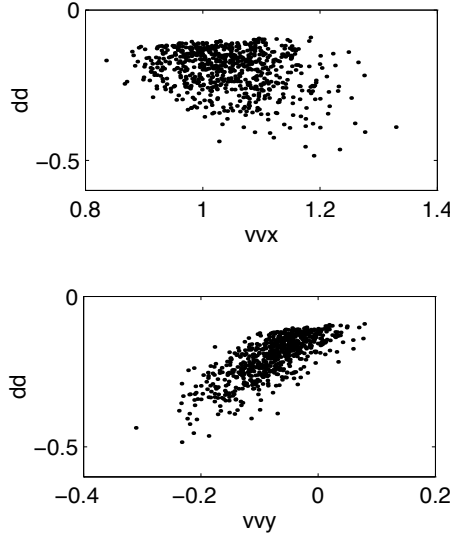


**Figure 6.** Dependence of the turnaround distance on the initial velocity of the reflected ion.

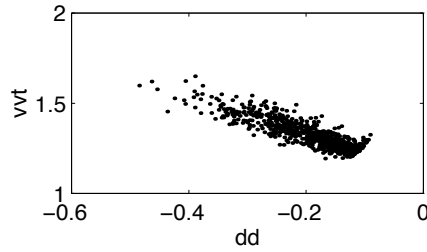
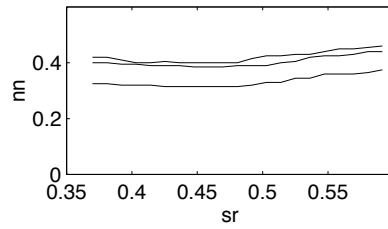


**Figure 7.** Correlation of the turnaround velocity with the turnaround distance.

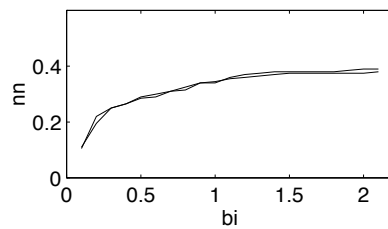
former case no additional potential is imposed, while in the latter the additional potential ensures  $e\varphi_t = 0.5(m_i V_u^2/2)$ . The added potential does not increase the effective potential crossed by the reflected ions noticeably but increases the electric field in the overshoot, thus increasing the effective shift velocity  $V_s$  and enhancing the reflection. One can see that the agreement between the exact numerical analysis and the theoretical model proposed in section 2 is excellent, taking into account the approximate character of the model. The discrepancy begins in the marginal region of small negative  $v_y$ . In Figure 5a almost 35% of ions are reflected. In Figure 5b this fraction increases up to 50%. Most of the reflected ions have relatively high initial peculiar velocities  $v_p = [(v_x - V_u)^2 + v_y^2]^{1/2}$ , and their gyrophases  $\theta$  ( $v_x - V_u = v_p \cos \theta$ ,  $v_y = v_p \sin \theta$ ) lie in the range  $220 \text{ deg} \lesssim \theta \lesssim 360 \text{ deg}$ , which is in good agreement with the results of hybrid simulations [see Burgess *et al.*, 1989, Figure 3].

Figure 6 presents the dependence of the turnaround distance of the reflected ion on its initial velocity. It is clearly seen that the turnaround distance is controlled mainly by  $v_y$ : the more negative the initial  $v_y$  is, the larger the turnaround distance. The number of reflected ions drops rapidly for  $x < -0.3(V_u/\Omega_i)$ , which is consistent with the chosen magnetic field profile and foot length. This distance corresponds to  $v_x \approx 1.2V_u$ ,  $v_y \approx -0.2V_u$ . For our parameters it is near  $(V_u + 2.15v_T, -2.15v_T)$ , as was assumed in section 2. In Figure 7 we show the correlation of the  $y$  component of the reflected-gyrating ion velocity  $u_{y,\text{turn}}$  at the turnaround point with the turnaround distance  $d$ . The dependence is almost linear, and the ion velocity is  $\approx 1.6V_u$  at the very upstream point, where reflected ions are observed, and  $\approx 1.5V_u$  at the edge of the foot, which is also in agreement with observations [Sckopke *et al.*, 1983].

Finally, we present the results of the analysis of the dependence of the reflection efficiency (fraction of reflected ions  $n_r/n_u$ ) on different shock parameters. Figure 8 shows the dependence of the reflected ion fraction on the potential at the ramp. The last one is obtained from (1) by simple scaling. The two upper curves are obtained for the case where we introduced additional potential and  $e\varphi_t/(m_i V_u^2/2) = 0.6$  and  $0.8$ . The increase of the efficiency with the increase of the additional potential is due to the enhancement of the overshoot electric field. The dependence on the ramp potential is weak. It should be noted that in all cases the potential is too low to stop the ions. Figure 9 shows the dependence of the reflection efficiency on the initial  $\beta_i$  found numerically and analytically from (17). As could be expected, the efficiency increases with the increase of  $\beta_i$ , since more ions with high  $v_\perp$  and large negative  $v_y$  are available. In Figure 10 we present the dependence of the reflected ion fraction on the magnetic compression ratio at the ramp  $B_r/B_u$ . The reflection efficiency



**Figure 8.** Dependence of the reflected ion fraction on the potential at the ramp. Two upper curves correspond to the cases when additional potential was introduced, so that the total cross-shock potential  $e\varphi_t/(m_i V_u^2/2) = 0.6$  and  $0.8$ .



**Figure 9.** Dependence of the reflected ion fraction on  $\beta_i$  (numerical and analytical).

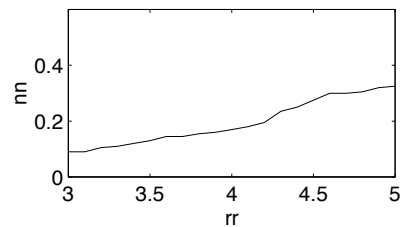


**Figure 10.** Dependence of the reflected ion fraction on the magnetic compression ratio  $B_r/B_u$ .

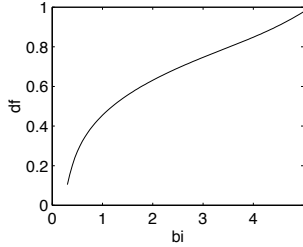


**Figure 11.** Dependence of the foot length on  $\beta_i$ .

rapidly increases with the increase of the ramp height, in complete agreement with (17). This behavior explains the observed anticorrelation of the reflection efficiency with the cross-shock potential, since the magnetic compression increases while the potential decreases with the increase of the Mach number. Figure 11 shows the dependence of the foot length, estimated as a turnaround distance of the ion with  $(v_x, v_y) = (V_u + 2.15v_T, -2.15v_T)$ , on  $\beta_i$ . The dependence is strong, and the foot lengths vary in a wide range. It should be noted, however, that  $\beta_i$ , other than  $\beta_i = 0.8$  used throughout the paper, are in general inconsistent with the chosen field structure. This is clearly seen from the fact that the obtained foot lengths differ greatly from our  $0.3(V_u/\Omega_i)$ . Still Figure 11 shows that the foot length may be sensitive to the ion temperature and expressions like those derived by Woods [1971] and Gosling and Thomsen [1985], and ignoring dependence on  $\beta_i$  can be misleading. That might be partially responsible for large deviations of the observed foot lengths from the predicted ones, found by Gosling and Thomsen [1985].

#### 4. 4. Discussion and Conclusions

As we have seen above, the details of the ion reflection process depend significantly on the shock structure and not only on the upstream and/or downstream parameters. Deviations of the actual shock structure from the model adopted here for the purposes of numerical analysis would give somewhat different quantitative results, which cannot be predicted unless we know the distribution of the electric and magnetic field in the foot, ramp, and overshoot. However, some tendencies can be predicted on the basis of the analytical consideration in section 2.

The increase of the change of the magnetic field over the foot  $B_f - B_u$  would increase the deflection in the negative  $y$  direction, thus supporting ion reflection. At the same time that would enhance the ion deceleration at the foot, thus reducing the ion gyration velocity just behind the ramp and acting against reflection. The same can be said about the influence of the ramp width: the wider the ramp, the stronger both the deviation along  $y$  axis and deceleration along  $x$  axis. In both cases the exact result of the competition would depend on the details of the profile, but since these changes act in both directions, one can expect weak dependence on both these factors.

The reflection process depends most strongly upon the magnetic compression ratio at the ramp, which determines the ratio of the ion gyration velocity to its drift velocity in the overshoot. The part of the cross-shock potential, applied at the ramp, plays mainly a negative role, reducing the ion gyration velocity at the downstream edge of the ramp. Presence of additional nonnegligible slowly varying electric field  $E_x < 0$  in the overshoot would further enhance the ion reflection, since it would increase the effective gyration velocity component  $v_y$  by the amount  $-E_x/B_o$ . Obviously, similar  $E_x > 0$  would suppress the ion reflection. The two effects of the electric field compete, and the result depends on the distribution of the potential and not only on the overall potential drop.

When  $\beta_i \gg 1$ , the cross-shock potential becomes able to decelerate part of the ions down to  $u_x = 0$  and reflect them electrostatically, that is, as predicted by the specular reflection model [Leroy, 1983]. These specularly reflected ions add to the nonspecularly reflected ions to form the complete reflected-gyrating ion distribution in the foot. Their contribution is significant only if  $\beta_i$  is sufficiently large or if the potential becomes high enough. (This effect can be enhanced by a strong increase of the magnetic field in the ramp.) On the other hand, increasing  $\beta_i$  increases also the number of nonspecularly reflected ions, so that specularly reflected ions would constitute only a part (and not a larger one) of the total number of reflected ions.

In conclusion, we studied analytically and numerically the details of ion reflection process at the shock front, paying particular attention to the role of the ramp crossing in the determination of what part of the incident ion distribution is reflected. We have shown that the reflection is due to the induced gyration in the overshoot and returning of the gyrating ions back to the ramp. We have derived an approximate reflection condition, which relates the initial velocities of the reflected ions to the cross-shock potential and the electric field in the overshoot, magnetic compression ratio, and integrated magnetic field (vector potential) over the foot and ramp. We have shown that the turnaround distance and therefore foot length differs from the foot length predicted by the specular reflection theory. It appears to be substantially smaller than expected for  $\beta_i \sim 1$ , which is consistent with both observations and earlier hybrid simulations. Therefore expressions found in the specular reflection model could give incorrect results when used for the determination of the shock velocity. We have

shown the correlation between the reflection efficiency and magnetic compression ratio and therefore Mach number. We have explained why strong ion reflection is possible, while the cross-shock potential is not sufficiently high.

**Acknowledgments.** The author is grateful to the referees for useful criticism. This research was supported by grant No. 94-00047 from the United States-Israel Binational Science Foundation (BSF), Jerusalem, Israel.

The Editor thanks two referees for their assistance in evaluating this paper.

## References

- Burgess, D., W.P. Wilkinson, and S.J. Schwartz, Ion distribution and thermalization at perpendicular and quasi-perpendicular supercritical collisionless shocks, *J. Geophys. Res.*, , 94, 8783, 1989.
- Goodrich, C.C., Numerical simulations of quasi-perpendicular collisionless shocks, in *Collisionless Shocks in the Heliosphere: Reviews of Current Research, Geophys. Monogr. Ser.*, vol. 35, edited by R.G. Stone and B.T. Tsurutani, p.153, AGU, Washington, D. C., 1985.
- Gosling, J.T., and A.E. Robson, Ion reflection, gyration, and dissipation at supercritical shocks, in *Collisionless Shocks in the Heliosphere: Reviews of Current Research, Geophys. Monogr. Ser.*, vol. 35, edited by R.G. Stone and B.T. Tsurutani, p.141, AGU, Washington, D. C., 1985.
- Gosling, J.T. and M.F. Thomsen, Specularly reflected ions, shock foot thicknesses, and shock velocity determinations in space, *J. Geophys. Res.*, , 90, 9893, 1985.
- Lee, M.A., V.D. Shapiro, and R.Z. Sagdeev, Pickup ion energization by shock surfing, *J. Geophys. Res.*, , in press, 1996.
- Leroy, M.M., Structure of perpendicular shocks in collisionless plasma, *Phys. Fluids*, 26, 2742, 1983.
- Liewer, P.C., V.K. Decyk, J.M. Dawson, and N. Lembègue, Numerical studies of electron dynamics in oblique quasi-perpendicular collisionless shock waves, *J. Geophys. Res.*, , 96, 9455, 1991.
- Schwartz, S.J., M.F. Thomsen, and J.T. Gosling, Ions upstream of the Earth's bow shock: A theoretical comparison of alternative source population, *J. Geophys. Res.*, , 88, 2039, 1983.
- Sckopke, N., G. Paschmann, S.J. Bame, J.T. Gosling, and C.T. Russell, Evolution of ion distributions across the nearly perpendicular bow shock: Specularly and nonspecularly reflected-gyrating ions, *J. Geophys. Res.*, , 88, 6121, 1983.
- Scudder, J.D., A. Mangeney, C. Lacombe, C.C. Harvey, T.L. Aggson, R.R. Anderson, J.T. Gosling, G. Paschmann, and C.T. Russell, The resolved layer of a collisionless, high  $\beta$ , supercritical, quasi-perpendicular shock wave, 1, Rankine-Hugoniot geometry, currents, and stationarity, *J. Geophys. Res.*, , 91, 11,019, 1986a.
- Scudder, J.D., A. Mangeney, C. Lacombe, and C.C. Harvey, The resolved layer of a collisionless, high  $\beta$ , supercritical, quasi-perpendicular shock wave, 2, Dissipative fluid hydrodynamics, *J. Geophys. Res.*, , 91, 11,053, 1986b.
- Wilkinson, W.P., and S.J. Schwartz, Parametric dependence of the density of specularly reflected ions at quasiperpendicular collisionless shocks, *Planet. Space Sci.*, 38, 419, 1990.
- Woods, L.C., On double structured, perpendicular, magneto-plasma shock waves, *J. Plasma Phys.*, 13, 281, 1971.
- Wygant, J.R., M. Bensadoun, and F.C. Mozer, Electric field measurements at subcritical, oblique bow shock crossings, *J. Geophys. Res.*, , 92, 11,109, 1987.
-